1. Agency Use Only *(Leave blank).*	2. Report Date. 1993	3. Report Type and Dates Covered. Final - Journal Article

4. Title and Subtitle.
Use of AVHRR data to verify a system for forecasting diurnal sea surface temperature variability

5. Funding Numbers.
Program Element No. 063704N
Project No. 0101
Task No. 100
Accession No. DN650757
Work Unit No. 93211F

6. Author(s).
J. D. Hawkins, R. M. Clancy*, and J. F. Price

7. Performing Organization Name(s) and Address(es).
Naval Research Laboratory
Ocean Science Branch
Stennis Space Center, MS 39529-5004

8. Performing Organization Report Number.
JA 321:049:91

9. Sponsoring/Monitoring Agency Name(s) and Address(es).
Space and Naval Warfare Systems Command
Washington, DC

10. Sponsoring/Monitoring Agency Report Number.
JA 321:049:91

11. Supplementary Notes.
*Fleet Numerical Oceanography Center, Monterey, CA
Published in Int. J. Remote Sensing, 1993.

12a. Distribution/Availability Statement.
Approved for public release; distribution is unlimited.

12b. Distribution Code.

13. Abstract *(Maximum 200 words).*

Forecasts from an operational system for predicting global diurnal sea surface temperature (SST) variability are compared against multichannel sea surface temperatures calculated from advanced very high resolution radiometer data from the NOAA-9 satellite. The forecast system consists of an upper-ocean model driven by heat fluxes and wind stresses from an operational global weather prediction model. Visual pattern correlations between observed and forecast diurnal changes in SST are generally favorable, indicating that the forecast system is useful. Some systematic deficiencies are also noted: the forecasts do not reproduce the surprisingly sharp boundaries of diurnal warming regions and underpredict the amplitude of the extreme warming events.

Original contains color plates: All DTIC reproductions will be in black and white

14. Subject Terms.
Remote sensing, thermodynamic ocean models, satellite sea surface temperature

15. Number of Pages.
11

16. Price Code.

17. Security Classification of Report.	18. Security Classification of This Page.	19. Security Classification of Abstract.	20. Limitation of Abstract.
Unclassified	Unclassified	Unclassified	SAR

DISCLAIMER NOTICE

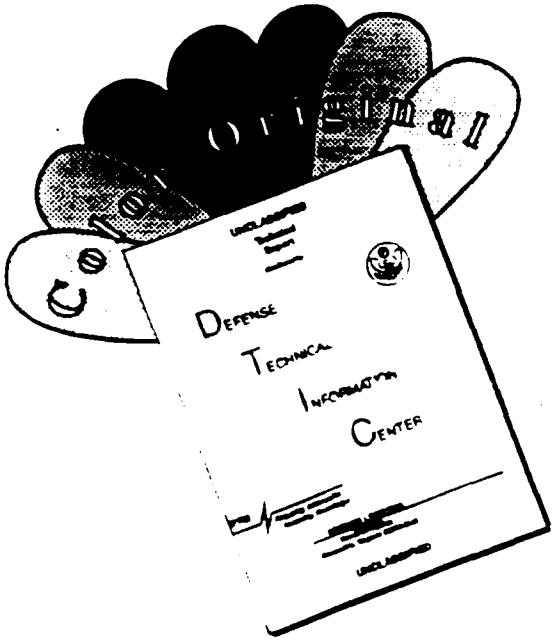

THIS DOCUMENT IS BEST QUALITY AVAILABLE. THE COPY FURNISHED TO DTIC CONTAINED A SIGNIFICANT NUMBER OF COLOR PAGES WHICH DO NOT REPRODUCE LEGIBLY ON BLACK AND WHITE MICROFICHE.

INT. J. REMOTE SENSING, 1993, VOL. 14, NO. 7, 1347-1357

Use of AVHRR data to verify a system for forecasting diurnal sea surface temperature variability

J. D. HAWKINS†

Ocean Sensing and Prediction Division, Naval Oceanographic and Atmospheric Research Laboratory, John C. Stennis Space Center, MS 39529, U.S.A.

R. M. CLANCY

Ocean Models Division, Fleet Numerical Oceanography Center, Monterey, CA 93943, U.S.A.

and J. F. PRICE

Woods Hole Oceanographic Institution, Woods Hole, MA 02543, U.S.A.

(Received 26 August 1991; in final form 2 June 1992)

Abstract. Forecasts from an operational system for predicting global diurnal sea surface temperature (SST) variability are compared against multichannel sea surface temperatures calculated from advanced very high resolution radiometer data from the NOAA-9 satellite. The forecast system consists of an upper-ocean model driven by heat fluxes and wind stresses from an operational global weather prediction model. Visual pattern correlations between observed and forecast diurnal changes in SST are generally favourable, indicating that the forecast system is useful. Some systematic deficiencies are also noted: the forecasts do not reproduce the surprisingly sharp boundaries of diurnal warming regions and underpredict the amplitude of the extreme warming events.

1. Introduction

Under conditions of light winds and relatively clear skies, temperatures and currents in the upper ocean undergo a diurnal cycle in response to insolation (Sverdrup *et al.* 1942, Stommel *et al.* 1969). An appreciable diurnal cycle can thus be expected to occur over about half of the world ocean—throughout the tropical and subtropical oceans over much of the year, and even at fairly high latitudes in the summer hemisphere.

The physics of this oceanic diurnal cycle are more complex than those of the corresponding terrestrial cycle because oceanic diurnal warming depends on two surface boundary conditions: the intensity of the net surface warming heat flux, which tends to inhibit vertical mixing by stabilizing the surface layer, and the

†Now at Naval Research Laboratory, Monterey, CA 93943, U.S.A.

strength of the wind stress, which produces vertical mixing (Price *et al.* 1986). For example, under conditions of strong heating and light or moderate winds, the wind mixing may be insufficient to mix the solar heat absorbed near the surface throughout the depth of the early morning mixed layer. As solar heating proceeds, the heat becomes trapped at progressively shallower depths, producing a transient thermocline at a 'trapping' depth, D, and a diurnal rise in sea surface temperature (SST), ΔT. The amplitude of ΔT, is proportional to H/D, where H is proportional to the net surface warming heat flux. A dependence of ΔT on H is expected but field studies have also shown that ΔT can be highly variable from day to day (or from region to region) because of wind-stress-induced variations of D (Tabata *et al.* 1965, Stramma *et al.* 1986).

The amplitude of sea surface warming can exceed 3°C on days when intense solar heating occurs along with very light winds. Such large transient sea surface temperature changes represent a significant noise source to satellite infrared studies of the mesoscale ocean circulation (Stramma *et al.* 1986) and tend to mask underlying features of oceanographic interest (Bohm *et al.* 1991). Typical values of diurnal warming are only a few tenths of a degree (e.g., Stommel *et al.* 1969, Price *et al.* 1986), but even this modest warming can be sufficient to degrade an acoustic surface duct. Moreover, the occurrence of even weak stable stratification in the upper-ocean temperature profile is a clear sign that vertical turbulent mixing has been largely cut off below the depth of the stratification. This stratification has an important effect on the wind-driven current, which develops a diurnal jet within the warm surface layer (Price *et al.* 1987). Over the long term, the repeated growth and decay of this diurnal jet contributes substantially to the mean profile of the wind-driven current.

In this article we report our efforts to make and to verify global forecasts of the oceanic diurnal cycles. These forecasts could be useful in a variety of contexts, including the identification of regions of diurnal warming to supplement the use and interpretation of satellite-derived SST data. In the broadest sense, the forecasts provide an immediate and verifiable link between surface heat fluxes and wind stresses, ocean thermodynamics, and the SST response of the ocean observable from satellites.

2. DOSL model formulation and implementation

The forecast system has two main components: (1) a simple model of the upper-ocean diurnal cycle, the Diurnal Ocean Surface Layer (DOSL) model, which is driven by (2) surface heat fluxes and wind stresses that are forecast by an operational numerical weather prediction model.

2.1. *Model formulation*

The DOSL model was formulated by Price *et al.* (1986) under the assumption that the principal mechanism of wind mixing is shear flow instability of wind-driven currents. Scale analysis and calibration against a full numerical model solution give the daily minimum trapping depth as approximately

$$D = 0{\cdot}45 \frac{S}{H^{1/2}} \left(\frac{\rho}{-\alpha g} \right)^{1/2} J(D/\lambda_2)^{-3/2} \tag{1}$$

and the magnitude of the surface warming as approximately

$$\Delta T = 1{\cdot}5\frac{H^{3/2}}{S}\left(\frac{-\alpha g}{c_p}\right)^{1/2} J(D/\lambda_2)^{3/2} \tag{2}$$

(see table 1 for full symbol definitions).

The function j models the effect of solar radiation penetration into the water column, which is presumed to follow a double exponential form,

$$I(z) = I(0)[I_1 \exp(-z/\lambda_1) + I_2 \exp(-z/\lambda_2)], \tag{3}$$

Table 1. Definitions.

Notation	Definition
$\alpha = \frac{1}{\rho}\frac{\delta\rho}{\delta T}$	thermal expansion coefficient for seawater
c	convection depth
$c_p = 3990\,\mathrm{J\,kg^{-1}\,C^{-1}}$	specific heat of seawater
ΔT	diurnal sea surface temperature warming
D	trapping depth of the diurnal thermal cycle
f	Coriolis parameter
$g = 9{\cdot}8\,\mathrm{m^2\,s^{-1}}$	acceleration of gravity
$H = P_q\frac{(\hat{I}+\bar{L})}{\rho_0 c_p}$	parameter proportional to the net heating of the ocean on a given day
I	instantaneous solar heat flux
$\hat{I}$	daily maximum value of the solar heat flux
I_1	fraction of solar flux at long wavelengths
$I_2 = 1 - I_1$	fraction of solar flux at short wavelengths
L	instantaneous loss of heat from the sea surface ($L<0$) due to latent + sensible + infrared heat fluxes
$\bar{L}$	average of L over the time of net downward surface heat flux
λ_1	solar extinction depth scale for long wavelengths
λ_2	solar extinction depth scale for short wavelengths
P_q	one-half the time interval over which the net surface heat flux is downward (i.e., $I+L>0$)
$P_\tau = \left[\frac{2-2\cos(fP_q)}{f}\right]$	the acceleration time scale for the diurnal current maximum
ρ	density of seawater
$\rho_0 = 1{\cdot}023\times10^3\,\mathrm{kg\,m^{-3}}$	reference density
$S = \frac{P_\tau\bar{\tau}}{\rho_0}$	parameter proportional to the net momentum imparted to the diurnal current maximum
τ	instantaneous surface wind stress
$\bar{\tau}$	surface wind stress averaged over the time of net downward surface heat flux
T	sea surface temperature
z	depth, positive downward

in which case,

$$J(D/\lambda_2)=\left[1-I_2\frac{\hat{I}-\bar{L}}{\bar{I}}\exp(-D/\lambda_2)\right]. \tag{4}$$

The amplitude of heating is represented by H, which is proportional to the net warming heat flux at the sea surface divided by the density and heat capacity of seawater. S is proportional to the volume transport of the wind-driven current in the diurnal thermocline. H can vary from 0 (no heating) to a maximum of possibly 6°C m on a day with the maximum possible insolation. S can vary from 0 (no wind) to almost any value. However, diurnal warming is significant only where S is less than about $1{\cdot}5\,m^2\,s^{-1}$, corresponding to a wind speed of about $8\,m\,s^{-1}$.

In the DOSL model, ΔT is proportional to $H^{3/2}$ rather than simply H because heating acts to stabilize the surface layer and thereby to reduce D. Conversely, wind mixing acts to increase D, so ΔT decreases with increasing S as S^{-1}. In general, the S (i.e., wind driven) dependence tends to dominate the day-to-day variation of ΔT.

Note that according to (2), ΔT becomes infinite if S vanishes. At the time the DOSL model was implemented for these tests, this obviously false limit was handled by requiring that ΔT not exceed 2·5°C and that D not be less than 0·5 m. Subsequent development of the scaling analysis provides a physically motivated treatment of this limiting case. If the surface wind stress becomes extremely weak, then wind-mixing may become less important than free convective mixing produced by the effect of heat loss from the surface. The scaling should then shift to a 'free convection limit' in which

$$\Delta T=\frac{\hat{I}(0)-\hat{I}(c)+\bar{L}}{c}\frac{P_q}{\rho_0 c_p}, \tag{5}$$

with the convection depth c (Dalu and Purini 1981) computed from

$$\frac{\hat{I}(0)-\hat{I}(c)+\bar{L}}{c}=\left.\frac{\partial I}{\partial z}\right|_c. \tag{6}$$

This depth remains finite as S vanishes, and the revised formulation gives plausible results for ΔT as well.

This model has been tested previously by comparison against high-quality *in situ* data from a moored buoy that made measurements of both SST and the meteorological variables required to estimate the surface heat flux and wind stress (Price *et al.* 1987). The results are summarized in figure 1, which shows ΔT as a function of H and S for 301 days, spanning two summers. The DOSL model gives the surface plotted in the background, which accounts for 77 per cent of the variance.

The DOSL model, equations (1–6), provides a compact and rather accurate basis for forecasting the ocean's diurnal cycle. Based on the analysis of Price *et al.* (1987) and provided that the surface heat fluxes and wind stresses can be forecast accurately, then the root-mean-square (rms) error between a pointwise measurement of ΔT and the forecast of the DOSL model should be about one-third the value of ΔT, or 0·1°C, whichever is larger. The bias in the forecasts should be less than 0.1°C.

2.2. *Model implementation at Fleet Numerical Oceanography Center (FNOC)*

For the results presented here, the DOSL model was forced by surface heat fluxes and winds provided at 6-hour temporal resolution by the Navy Operational Global Atmospheric Prediction System (NOGAPS) model (Hogan and Rosmond

1991, Rosmond 1992). The wind-speed-dependent drag coefficient of Garratt (1977) was used to calculate surface wind stresses from the NOGAPS 19·5 m winds. In calculating H and S, the algorithms of Clancy and Pollak (1983) were used to interpolate the surface heat fluxes and wind stresses between the 6-hourly values provided by NOGAPS, ensuring an accurate representation of the diurnal insolation.

The most likely source of error in a DOSL forecast is uncertainty in H and S, rather than an error in the ocean component of the forecast system. The probable error on a pointwise daily forecast of H or S is very difficult to assess quantitatively, but the global-average errors in these quantities are on the order of 0·2–0·5°C m and 0·5–1·0 $m^2 s^{-1}$ (Fleet Numerical Oceanography Center 1990, Rosmond 1992). The hypothesis we test qualitatively in this paper is that the surface heat fluxes and wind stresses from NOGAPS, in conjunction with the DOSL model, are accurate enough to forecast large-scale patterns of ΔT with useful skill.

For the cases used in this study, the DOSL model is run on the FNOC 63 by 63 polar stereographic grids of the Northern Hemisphere and Southern Hemisphere. These grids have resolution ranging from about 200 km in the tropics to about 360 km in the high latitudes. The model forecasts are then interpolated to a 2·5° latitude by 2·5° longitude grid for output and display.

An example DOSL forecast and corresponding FNOC surface weather chart are

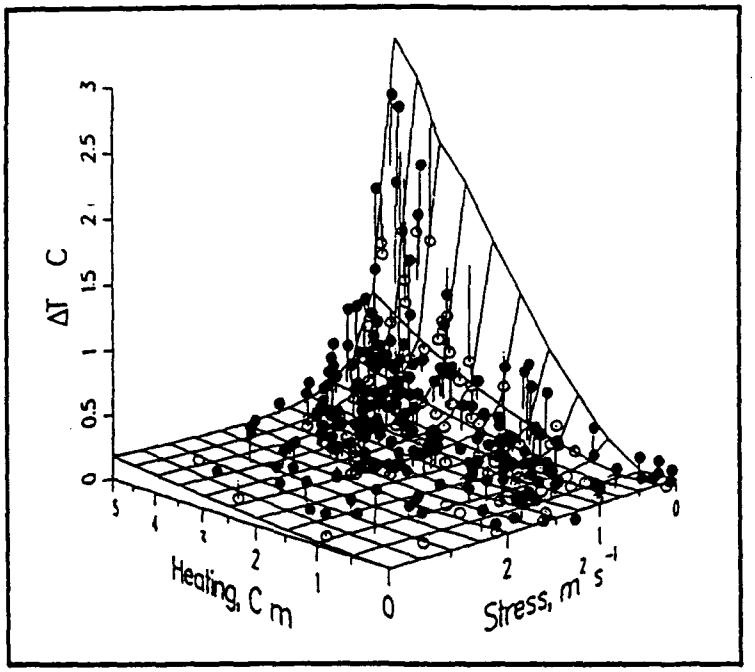

Figure 1. Predicted and observed ΔT as a function of H and S based on data from a buoy moored at 34° N, 70° W. The three-dimensional surface represents the warming predicted by the DOSL model when forced with H and S obtained from the buoy observations, and the black and white dots depict the observed values of ΔT. The vertical lines from each dot show the error between the DOSL model prediction and the observed warming. The black (white) dots indicate instances where the DOSL model underpredicted (overpredicted) the observed warming. From Price *et al.* (1987).

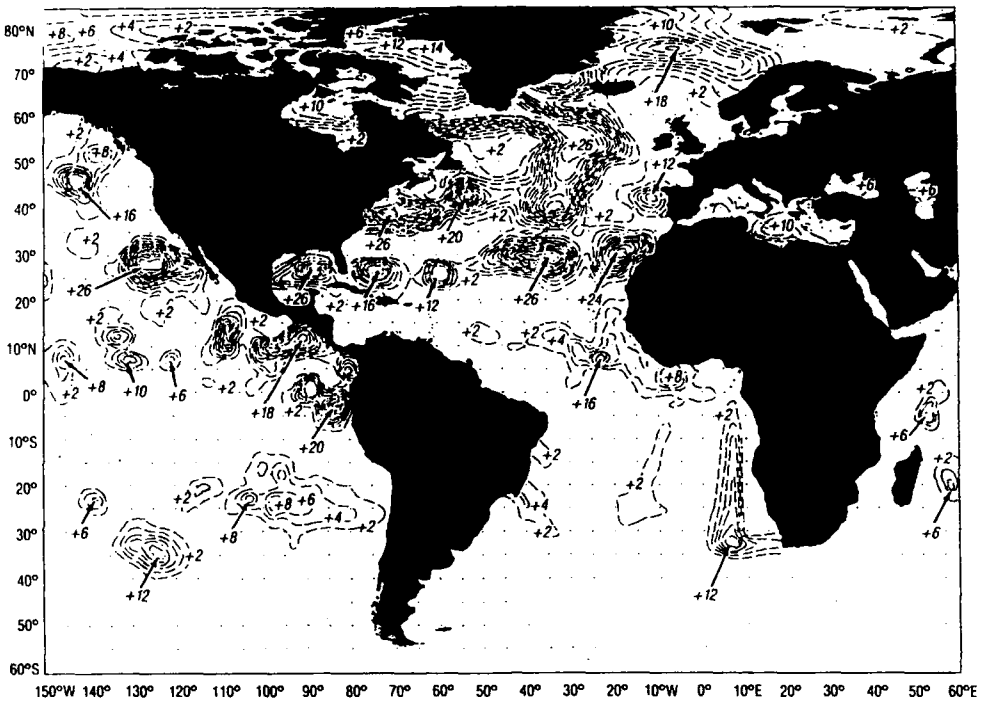

Figure 2. The ΔT predicted for 6 August 1987 by the DOSL model implemented at FNOC. The contour interval is 0·2°C and the labels are in tenths of degrees Celsius.

shown in figures 2 and 3 for 6 August 1987. Note the marked asymmetry about the equator, with much stronger and more extensive diurnal warming predicted for the Northern, or summer, Hemisphere. There are about 10 regions with predicted warming of 2°C or more in the Northern Hemisphere. These regions are typically 10–20° of longitude in width, and all correspond to areas of light winds and little or no cloud cover. For example, extensive afternoon warming is predicted beneath the Bermuda–Azores high, which covers most of the subtropical North Atlantic. Diurnal warming cycles may be quasi-steady for several days or a week in this region. However, in other regions, diurnal warming events are much more variable and intermittent. Most notable is the region in the eastern Pacific off southern Mexico, where significant diurnal warming is predicted in the saddle region between two rapidly moving tropical storms.

3. Satellite SST data

We used data from the AVHRR aboard the NOAA-9 satellite to calculate multichannel sea surface temperatures (MCSSTs) for verification of the forecast system. We calculated MCSSTs from day-time and night-time passes of the satellite, and used the day–night differences in this data to produce patterns of diurnal SST warming events for comparison with the model predictions. Note that the MCSSTs have an rms error of about 0·7°C (Strong and McClain 1985).

The data were processed as follows:

(*a*) NOAA-9 channels 4 and 5 data were calibrated and earth located using interactive digital image processing software (Hawkins *et al.* 1985).

(*b*) Earth location was fine tuned using appropriate landmarks, resulting in registration accuracies of 2 pixels or better.

(*c*) Conservative cloud tests, using data from only channels 4 and 5, were applied to eliminate cloud-contaminated pixels.

(*d*) MCSSTs were calculated for all pixels that were cloud-free in both the day-time and night-time passes. Night-time MCSSTs were then subtracted from the corresponding day-time values to produce day–night difference images, which then were false coloured in 0·5°C increments with clouds masked in dark grey.

4. Case studies

More than 100 AVHRR digital images from the summers of 1986 and 1987 in regions favourable for significant diurnal SST variability were processed into day–night MCSST images. Finding cloud-free conditions in consecutive day/night images over large areas proved difficult; we were forced to eliminate most of the data from further consideration, even though cloud-free bits and pieces verified well with the DOSL predictions (Hawkins *et al.* 1990). August was the most favourable month for this test in that five day–night image pairs in the North Atlantic provided a relatively unobstructed view of diurnal SST variability. Three of these five cases are presented below.

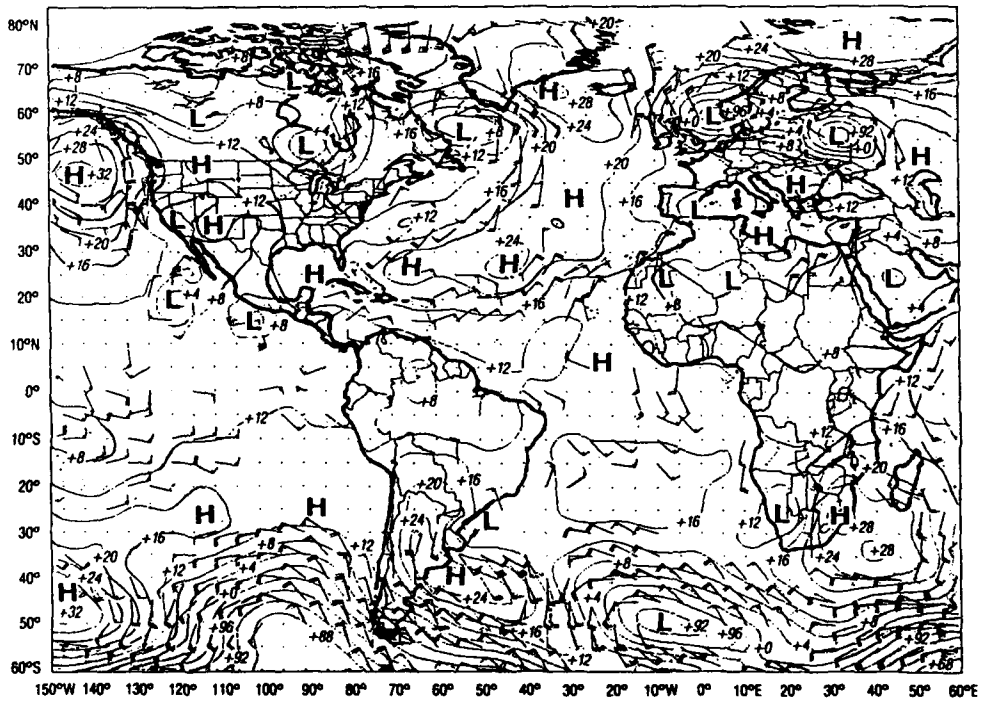

Figure 3. FNOC surface weather analysis for 12.00 GMT, 6 August 1987. Contours are of surface pressure with a 4 mb contour interval (add 1000 to all values < 50 and 900 to all values > 50 to obtain the contour label in mb). Wind barbs depict winds at 19·5 m height for regions where the winds equal or exceed 15 kt (approximately 7 ms^{-1}).

4.1. *16 August 1986*

The day–night difference image off the northwestern coast of Africa (figure 4) shows diurnal warming in excess of 0·5°C over a large triangular-shaped region that spans more than 20° of latitude and 30° of longitude. Several areas of diurnal SST warming in the range of 3–4°C are evident, including a narrow south-west/north-east-oriented band of intense warming between about 29° N, 19° W and 32° N, 13° W. This very warm water contributes to a substantial SST gradient perpendicular to the northwestern African coast.

The DOSL forecast of ΔT is displayed as white contours on figure 4, which shows that the forecast pattern is much like that observed in the satellite imagery. The south-west to north-east band of intense warming just off the coast is well represented by a DOSL contour in excess of 1°C. The model forecast correctly predicts warming along 25°N across a wide expanse. Two large pockets of 2·5°C warming occur at 26° N, 25° W and 32° N, 35° W in the DOSL forecast, with the westernmost one agreeing well with the day–night MCSST imagery. The eastern maximum is slightly displaced to the south east.

4.2. *17 August 1986*

The following day, 17 August 1986, also exhibits strong diurnal warming patterns off the northwestern coast of Africa, although without the intensity evident in the previous case. The day–night difference image and the DOSL prediction are shown in figure 5. This figure reveals a broad region of observed warming between about 20° N and 35° N, which is in general agreement with the DOSL prediction. The eastern segment is not quite as sharply defined as on the previous day, but some cloud-free pixels have likely been masked out due to sunglint near 30° N, 15° W. The regions of DOSL-predicted maxima near 30° N, 18° W and 33° N, 32° W are partially obscured by clouds, so comparisons there are difficult. However, the imagery clearly indicates several zones of 3°–4°C warming near 28° N, 38° W, between the two westernmost DOSL-predicted maxima.

4.3. *6 August 1987*

This case is for the same day as the DOSL model and surface weather charts presented in figures 2 and 3, and provides a detailed look at the diurnal SST warming in the region of the Bermuda–Azores high (figure 6). The DOSL forecast depicts the location and orientation of the observed warming centred near 29° N, 40° W very well, but displaces the model pattern slightly to the east and too broadly in north–south extent. Much of the northern part of the image is obscured by clouds, but the model fails to depict the observed maxima in warming at 34° N, 43° W.

5. Summary and remarks

As shown by the work of Cornillon and Stramma (1985), Stramma *et al.* (1986), and many others, diurnal sea surface temperature variability is widespread. It is a direct result of insolation and is strongly modulated by the magnitude of the surface wind stress. The diurnal cycle often dominates short-term variability in upper-ocean thermal stratification (Price *et al.* 1986) and is an important consideration in the use and interpretation of satellite SST data, as it tends to mask underlying features of oceanographic interest (Bohm *et al.* 1991). Because the diurnal SST response is a nonlinear function of the wind speed, smoothly varying patterns of the synoptic

Figure 4.

Figure 5.

Figure 4. Day–night MCSST difference image for 16 August 1986 colour-coded according to the scale at the top. Areas obscured by cloud or sunglint are masked out in dark grey. White contour lines are the corresponding ΔT predicted by the DOSL model (contours displayed are 0·2, 0·5, 1·0, 1·5, 2·0, and 2·5°C).

Figure 5. Day–night MCSST difference image for 17 August 1986 colour-coded according to the scale at the top. Areas obscured by cloud or sunglint are masked out in dark grey. White contour lines are the corresponding ΔT predicted by the DOSL model (contours displayed are 0·2, 0·5, 1·0, 1·5, 2·0, and 2·5°C).

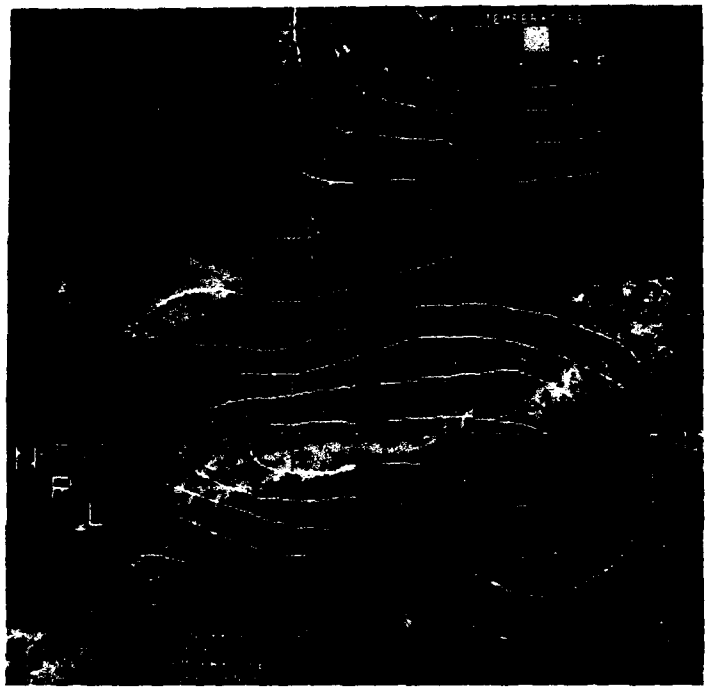

Figure 6. Day–night MCSST difference image for 6 August 1987 colour-coded according to the scale at the top. Areas obscured by cloud or sunglint are masked out in dark grey. White contour lines are the corresponding ΔT predicted by the DOSL model (contours displayed are 0·2, 0·5, 1·0, 1·5, 2·0, and 2·5°C).

wind field tend to produce comparatively sharp gradients in diurnal SST features. These sharp horizontal gradients are easily misinterpreted as current or water-mass boundaries.

The DOSL model relates the amplitude of the upper ocean's diurnal response to the surface heat flux and wind stress acting on the ocean. Price *et al.* (1987) verified this model using observed heat fluxes, winds, and SSTs at a moored buoy. We presented results from an operational global implementation of the DOSL model at the U.S. Navy's FNOC, and verified its forecasts with SSTs derived from satellite infrared data. In its implementation at FNOC the DOSL model is driven with surface heat fluxes and wind stresses provided by the NOGAPS numerical weather prediction model. Thus verification of the DOSL predictions is an indirect verification of the surface heat fluxes and wind stresses from the NOGAPS model.

The DOSL model gives plausible forecasts of the large-scale patterns of diurnal SST warming, as evidenced by the limited set of case studies presented here. These results also point out obvious deficiencies. The forecast fields do not have sufficient horizontal resolution to define the rather sharp boundaries of the observed diurnal warming events, and the forecasts underpredict the maximum warmings. Planned upgrades will address these shortcomings by doubling the spatial resolution of both the DOSL and NOGAPS models and by implementing the free-convection limit in the DOSL model to handle the case of vanishing wind stress. Surface heat fluxes in the NOGAPS model have been improved since the time of this study and will continue to be improved. Given reliable forecasts from the DOSL model, satellite

oceanographers could remove or suppress diurnal variability in SST imagery and thus have a better view of mesoscale ocean features.

Acknowledgments

The authors acknowledge the support of D. May and F. Abell, Jr, in extracting and processing the satellite imagery used in this study. This work was supported by the Office of Naval Research, the Chief of Naval Operations (OP-096) and the Space and Naval Warfare Systems Command, under program element 63704N, Lt Cdr W. Cook, Program Manager. NOARL Contribution JA 321:049:91.

References

BOHM, E., MARULLO, S., and SANTOLERI, R., 1991, AVHRR visible–IR detection of diurnal warming events in the western Mediterranean Sea. *International Journal of Remote Sensing*, **12**, 695–701.

CLANCY, R. M., and POLLAK, K. D., 1983, A real-time synoptic ocean thermal analysis/forecast system. *Progress in Oceanography*, **12**, 383–424.

CORNILLON, P., and STRAMMA, L., 1985, The distribution of diurnal sea surface warming events in the western Sargasso Sea. *Journal of Geophysical Research*, **90**, 11811–11815.

DALU, G. A., and PURINI, R., 1981, The diurnal thermocline due to buoyant convection. *Quarterly Journal of the Royal Meteorological Society*, **108**, 929–935.

FLEET NUMERICAL OCEANOGRAPHY CENTER, 1990, Quarterly performance summary. Technical Note, Volume 5 Number 3, Fleet Numerical Oceanography Center, Monterey, CA 93943.

GARRATT, J. R., 1977, Review of drag coefficients over oceans and continents. *Monthly Weather Review*, **105**, 915–929.

HAWKINS, J. D., ARNONE, B., ARTHUR, D., DANIELS, C., HOLYER, R., LA VIOLETTE, P., LYBANON, M., MCKENDRICK, J., MITCHELL, J., MOODY, B., PECKINPAUGH, S., PRESSMAN, A., SCHMIDT, J., SMITH, P., and STEPHENSON, G., 1985, Remote sensing at NORDA. *Transactions of the American Geophysical Union*, **66**, 482–483.

HAWKINS, J. D., MAY, D. A., and ABELL, F., 1990, Diurnal ocean surface layer model validation. NOARL Report 3, Naval Oceanographic and Atmospheric Research Laboratory, Stennis Space Center, MS 39529.

HOGAN, T. F., and ROSMOND, 1991, The description of the Navy Operational Global Atmospheric Prediction System's spectral forecast model. *Monthly Weather Review*, **119**, 1786-1815.

PRICE, J. F., WELLER, R. A., and PINKEL, R., 1986, Diurnal cycling: Observations and models of the upper ocean response to diurnal heating, cooling, and wind mixing. *Journal of Geophysical Research*, **91**, 8411–8427.

PRICE, J. F., WELLER, R. A., BOWERS, C. M., and BRISCOE, M. G., 1987, Diurnal response of sea surface temperature observed at the long-term upper ocean study (34° N, 70° W) in the Sargasso Sea. *Journal of Geophysical Research*, **92**, 14480–14490.

ROSMOND, T. E., 1992, The design and testing of the Navy Operational Global Atmospheric Prediction System. *Weather and Forecasting*, **7**, 262-272.

STOMMEL, H., SAUNDERS, K., SIMMONS, W., and COOPER, J., 1969, Observations of the diurnal thermocline. *Deep Sea Research*, **16**, 269–284.

STRAMMA, L., CORNILLON, P., WELLER, R., PRICE, J., and BRISCOE, M., 1986, Large diurnal sea surface temperature variability: Satellite and in situ measurements. *Journal of Physical Oceanography*, **16**, 827–837.

STRONG, A., and MCCLAIN, P., 1985, Improved ocean surface temperature from space-comparison with drifting buoys. *Bulletin of the American Meteorological Society*, **65**, 138–142.

SVERDRUP, H. U., JOHNSON, M. W., and FLEMING, R. H., 1942, *The Oceans, Their Physics, Chemistry and Biology* (Englewood Cliff, N.J.: Prentice Hall).

TABATA, S., BOSTON, N. E. J., and BOYCE, F. M., 1965, The relation between wind speed and summer isothermal surface layer of water at Ocean Station P in the eastern subarctic North Pacific. *Journal of Geophysical Research*, **70**, 3867–3878.